ACS Photonics

pubs.acs.org/journal/apchd5

Article

Two-Dimensional Platinum Diselenide Waveguide-Integrated Infrared Photodetectors

Shayan Parhizkar, Maximilian Prechtl, Anna Lena Giesecke, Stephan Suckow,* Sophia Wahl, Sebastian Lukas, Oliver Hartwig, Nour Negm, Arne Quellmalz, Kristinn Gylfason, Daniel Schall, Matthias Wuttig, Georg S. Duesberg, and Max C. Lemme*

Cite This: *ACS Photonics* 2022, 9, 859–867

Read Online

ACCESS | Metrics & More | Article Recommendations | Supporting Information

ABSTRACT: Low-cost, easily integrable photodetectors (PDs) for silicon (Si) photonics are still a bottleneck for photonic-integrated circuits (PICs), especially for wavelengths above 1.8 μm. Multilayered platinum diselenide ($PtSe_2$) is a semi-metallic two-dimensional (2D) material that can be synthesized below 450 °C. We integrate $PtSe_2$-based PDs directly by conformal growth on Si waveguides. The PDs operate at 1550 nm wavelength with a maximum responsivity of 11 mA/W and response times below 8.4 μs. Fourier-transform IR spectroscopy in the wavelength range from 1.25 to 28 μm indicates the suitability of $PtSe_2$ for PDs far into the IR wavelength range. Our $PtSe_2$ PDs integrated by direct growth outperform $PtSe_2$ PDs manufactured by standard 2D layer transfer. The combination of IR responsivity, chemical stability, selective and conformal growth at low temperatures, and the potential for high carrier mobility makes $PtSe_2$ an attractive 2D material for optoelectronics and PICs.

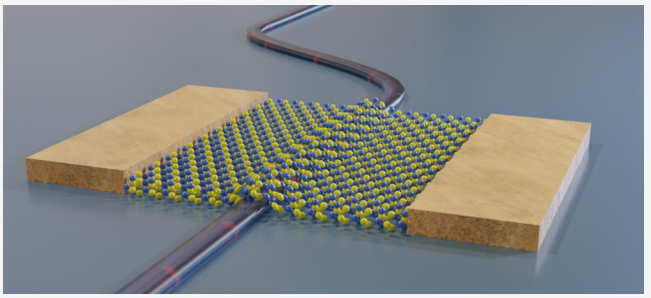

KEYWORDS: *platinum diselenide, photodetector, silicon photonics, two-dimensional materials, infrared*

INTRODUCTION

Photonic-integrated circuits (PICs) are maturing as a platform for applications in telecommunications, spectroscopy, diagnostics, biomedical imaging, and gas sensing.[1] PICs tailored for these applications typically rely on infrared (IR) photodetectors (PDs) that are coupled to waveguides and that function as essential components for optoelectronic signal conversion. PDs for the near-IR wavelength range are mainly based on widely used semiconductors such as Si[2] and Ge.[3] Mid-IR PDs are typically made from compound semiconductors such as InGaAs[4] and HgCdTe,[5] with the downside of higher manufacturing cost and the necessity of cryogenic temperature operating conditions. However, a key requirement toward the broad applicability of PICs is the integrability of IR PDs on photonic waveguides. This is not fulfilled by commercial manufacturing methods for the conventional materials because their high deposition and (epitaxial) growth temperatures are not compatible with PIC thermal budgets. This creates a demand for IR PDs with high manufacturability at low-temperature budgets.

Two-dimensional (2D) materials have attracted tremendous attention in the optoelectronic field due to their broadband optical absorption, high carrier mobility, mechanical flexibility, and ease of integration.[6−10] Quantum confinement in 2D materials in the direction perpendicular to their 2D plane leads to novel physical properties that distinguish them from their bulk materials.[11] A wide range of devices such as broadband PDs,[12] modulators,[13,14] lasers,[15] light-emitting diodes,[16] phototransistors,[17−19] and avalanche photodiodes[20] have been demonstrated to emphasize the advantages of 2D materials for optoelectronics.

In particular, the zero-bandgap material graphene has been used to demonstrate high-performance integrated PDs and modulators in the IR region.[21−25] However, graphene requires a layer-transfer process[26,27] because its growth is limited to a few substrate materials and requires high temperatures. 2D black phosphorus is also suitable as an IR PD[28,29] material that can be transferred onto waveguides[30,31] but has the drawback that it is not entirely stable under ambient conditions.[32] Platinum diselenide ($PtSe_2$) is a transition metal dichalcogenide (TMD) with an octahedral lattice structure that is semiconducting with an indirect bandgap of 1.2 eV as a monolayer. As a multilayer material, it becomes semi-metallic.[33] This semi-metallic nature of layered $PtSe_2$ allows

Received: October 6, 2021
Published: March 4, 2022

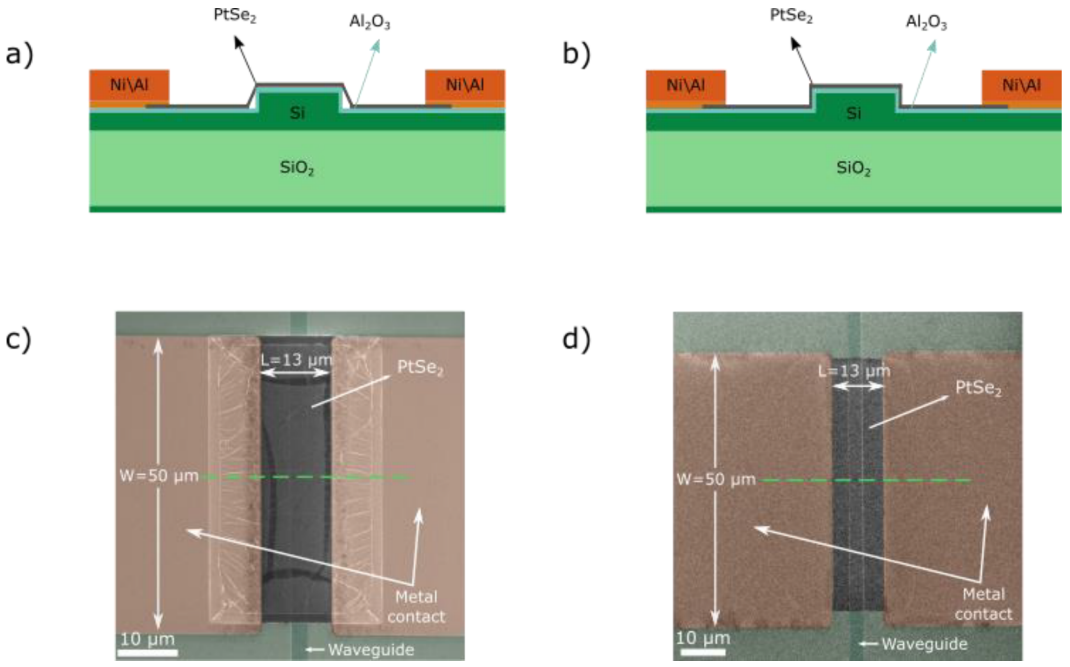

Figure 1. Schematic cross sections and false color SEM micrographs of transferred (a,c) and directly grown (b,d) $PtSe_2$ PDs on silicon waveguides. The wrinkles visible in the SEM image in (c) are due to wet transfer and consequently absent in (d). The green dashed lines indicate the direction of the cross sections in (a,b).

its use for broadband IR photodetection in a similar way to graphene.[34−36] In addition, $PtSe_2$ is stable in air and has a high charge carrier mobility compared to other TMDs, with theoretically predicted values of more than 1000 cm^2/Vs,[37,38] and has a piezoresistive gauge factor of up to −85.[39−41] A major advantage of $PtSe_2$ is the possibility of direct, large-scale growth on various substrates at temperatures below 450 °C using the thermally assisted conversion (TAC) technique.[34,40,42,43] In combination with the potential for selective and conformal deposition,[44] $PtSe_2$ is suitable for back-end-of-line (BEOL) integration on electronic and photonic wafers.

In this work, we demonstrate the use of layered $PtSe_2$ as an integrated IR PD on Si photonic waveguides. We compare the device performance and material quality of a direct growth integration approach with a wet layer-transfer technique through analytical, electrical, and optical characterization.

EXPERIMENTAL SECTION

The $PtSe_2$ PDs were realized on rib waveguides with a 50 nm step height on silicon-on-insulator (SOI) substrates. Optical access is provided through two grating couplers that are optimized for a wavelength of 1550 nm and transverse electric (TE) polarization. We fabricated two sets of samples: one using direct growth and another using a wet transfer method of the $PtSe_2$ layers. For the first set, a 10.8 nm thick layer of prepatterned sputtered platinum (Pt) was converted into a 27 nm thick layered film of $PtSe_2$ directly on the waveguides using TAC.[34] Pt is a highly reactive material. A thin barrier layer of Al_2O_3 was therefore deposited with atomic layer deposition (ALD) to protect the waveguides and grating couplers from the reaction of Pt with the top Si photonic layer during the TAC growth. For the second set of samples, $PtSe_2$ films of 7.6, 13.7, and 23.5 nm thickness were grown by TAC on separate silicon substrates with a 90 nm thermal silicon oxide (SiO_2) layer and were wet-transferred onto the Si waveguides (see Methods for details). The thicknesses of the $PtSe_2$ films were measured by atomic force microscopy (AFM) (Supporting Information). In both sample sets, the $PtSe_2$ patches came in contact with nickel/aluminum (Ni/Al) electrodes that had a distance of 5 μm to the waveguides. The width of the $PtSe_2$ channels on the waveguide along the light propagation direction for all PDs is W = 50 μm. Schematic cross sections of the integrated PDs and scanning electron microscopy (SEM) images of a transferred and a directly grown PD are shown in Figure 1a−d.

The topography of the $PtSe_2$ films around the waveguides is different for the two different integration methods. The wet transfer method presumably leads to small air gaps around the sidewalls of the Si waveguides, which is known from graphene devices,[45] as indicated schematically in Figure 1a. With the wet transfer process, the conformal coverage around the waveguide is not possible because of the limited flexibility of the transfer polymer. In addition, wrinkles in the $PtSe_2$ layer are visible that result from the wet transfer process (Figure 1c). In the case of directly grown $PtSe_2$, the sputtered Pt covers the sidewalls of the waveguides, which results in a conformal $PtSe_2$ film around the waveguide (Figure 1b,d). This feature underlines the advantage of direct 2D material growth over layer transfer, which often requires additional planarization processes to avoid tearing of the 2D films at the sharp edges of the waveguides[24,46] and reduces the strain effects arising from the bending of the 2D films over the waveguides.[47,48]

Raman spectroscopy was carried out on all devices to confirm the successful formation and quality of $PtSe_2$ layers after fabrication (Figure 2a). The spectra of various $PtSe_2$ films on the SOI substrate exhibit two characteristic peaks at approximately 177 and 206 cm^{-1}, which represent the E_g and A_{1g} modes of layered $PtSe_2$, respectively.[49] The E_g peak originates from the in-plane vibration of selenium (Se) atoms and the A_{1g} peak is caused by the out-of-plane vibration of Se atoms. As the number of $PtSe_2$ layers increases, a red shift in the position of both peaks and an increase in the intensity ratio

https://doi.org/10.1021/acsphotonics.1c01517
ACS Photonics 2022, 9, 859−867

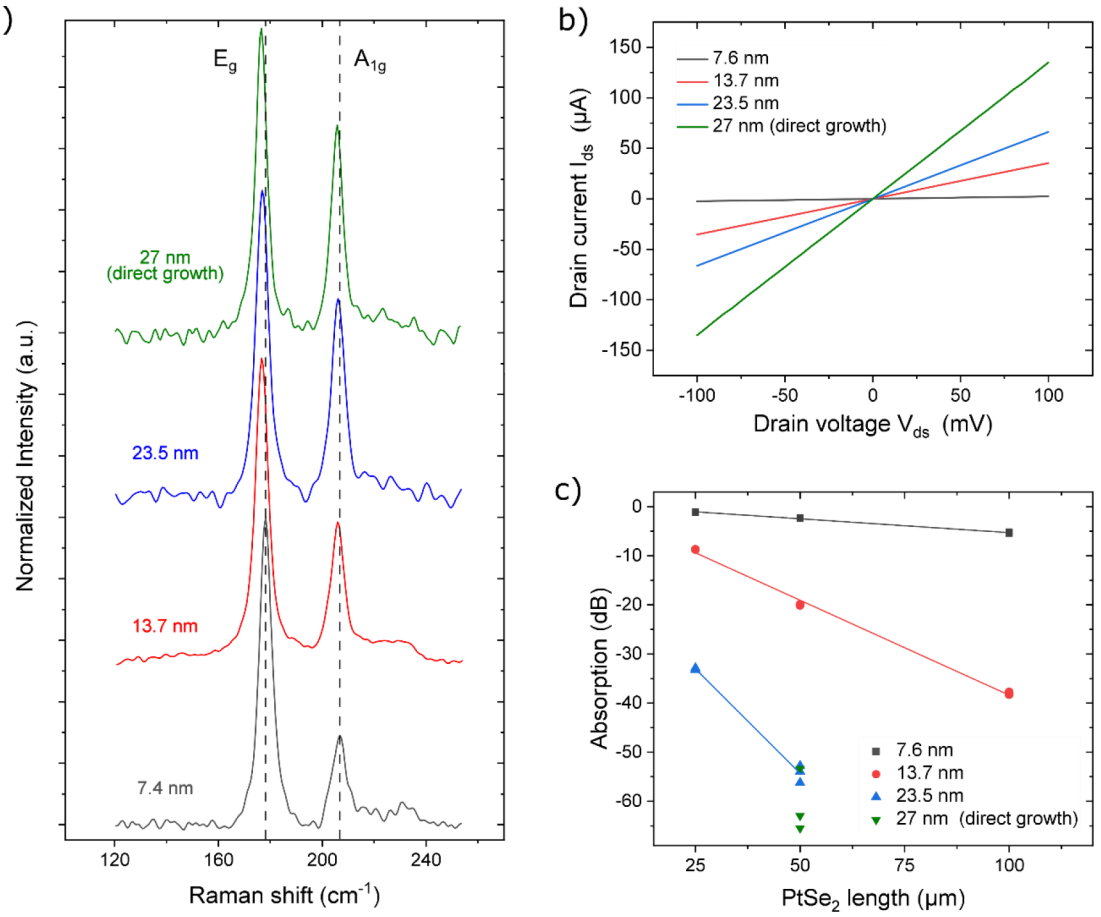

Figure 2. (a) Raman spectra of $PtSe_2$ with different thicknesses of transferred $PtSe_2$ (gray, red, and blue lines) and direct growth (green line). The spectra represent the average of area scans. They were recorded with an integration time of 1 s and averaged over 10 accumulations. (b) Drain current (I_{ds}) as a function of drain-source voltage (V_{ds}) for different $PtSe_2$ PDs. (c) Evanescent field absorption of $PtSe_2$ films on the waveguide at 1550 nm wavelength. The absorption per propagation distance for 7.6, 13.7, 23.5, and 27 nm thick (directly grown) $PtSe_2$ is 0.06, 0.38, 0.85, and 1.2 dB/μm, respectively.

of the two peaks $I(A_{1g})/I(E_g)$ are observed. This behavior can be explained by an increasing out-of-plane contribution due to an increase of van der Waals interactions between the layers.[49] The full width at half-maximum (FWHM) of the E_g peak indicates the material quality of $PtSe_2$.[50,51] For high-quality TAC-grown $PtSe_2$ films, the FWHM is smaller than 5 cm^{-1}.[41] For our samples with a directly grown $PtSe_2$ film, the FWHM of the E_g peak is 4.8 cm^{-1}. For the samples with transferred $PtSe_2$, this value varies between 5.1 and 5.6 cm^{-1}. In both cases, these values indicate a high material quality which is sufficient for device integration.[41] We note that there is still a quality gap between highly crystalline exfoliated films and thin films grown by various techniques.

Current−voltage (IV) measurements of the $PtSe_2$ detectors with different thicknesses show near-linear behavior for small source-drain voltages, which indicates semi-metallic characteristics of the $PtSe_2$ films and Ohmic contacts to the Ni/Al electrodes (Figure 2b). The resistance of $PtSe_2$ decreases with increasing layer thickness. The directly grown $PtSe_2$ layer exhibits similar properties to the transferred layers. However, as the drain voltages are increased, the IV curves clearly deviate from the linear behavior, which indicates the existence of back-to-back Schottky barriers at the interfaces (Figure S3 in the Supporting Information). This is confirmed by taking the derivative of the IV curves, which show that a weak nonlinearity is also present for smaller bias voltages and slightly stronger for thinner films (Figure S4 in the Supporting Information). The latter is in line with previous reports that have observed semiconducting behavior for thin TAC films.[43] These films are still multilayer films, and the reason of their semiconducting behavior is under discussion because in theory, the semi-metal to semiconductor transition should happen predominantly for monolayer films.[52] The signatures of Schottky barriers at the contact interfaces of thicker films, which are expected to be semi-metallic, have been explained by the coexistence of semi-metallic and semiconducting domains in the TAC-grown films.[53] Nevertheless, the resistivities of nickel/aluminum contacts to $PtSe_2$ films have been measured with the transfer length method (TLM) to vary between 0.7 and 2 kΩ μm for the same batch of samples in a previous study.[41] Such values allow us to neglect the effect of the metal contacts on the total device resistance for our purposes and to use the two-probe configuration for further analysis. This is an important observation because the direct growth process includes Pt deposition and TAC on the sidewalls and at the edges and corners, which is the key enabler for the direct integration of $PtSe_2$ on photonic structures.

The light−matter interaction of the $PtSe_2$ films was characterized for IR light with a wavelength of λ = 1550 nm that was coupled into one grating coupler through a single-

https://doi.org/10.1021/acsphotonics.1c01517
ACS Photonics 2022, 9, 859−867

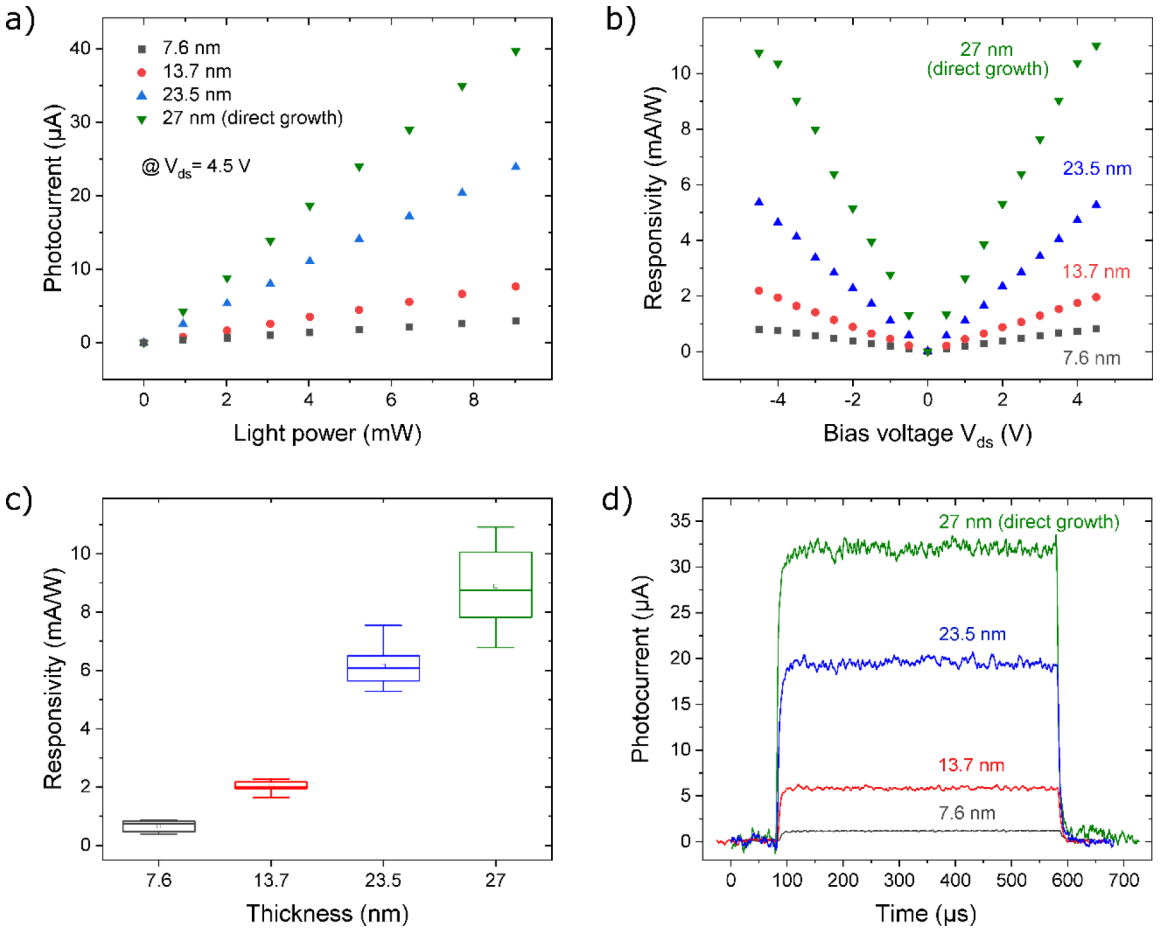

Figure 3. Optical measurements of $PtSe_2$ PDs. All devices are 50 μm wide along the waveguide direction. (a) Photocurrent as a function of light power at 4.5 V bias voltage. All $PtSe_2$ PDs respond linearly to the light power. (b) Responsivity vs bias voltage calculated at 9 mW laser output power. (c) Box plot of responsivities for different thickness $PtSe_2$ PDs measured at 4.5 V applied bias. (d) Time-resolved measurement of the $PtSe_2$ PDs at 8 mW optical power and 4.5 V bias voltage. The measured rise and fall times for the devices are between 8 and 13 μs.

Table 1. Summary of the Different $PtSe_2$ PDs; Maximum Responsivity, NPDR, and Rise/Fall Time of All the PDs

$PtSe_2$	thickness (nm)[a]	number of layers (estimate)	absorption (dB/μm)	max responsivity (mA/W)[b]	NPDR (W^{-1})[b]	rise/fall time (μs)[b]
sample A: grown on Si/SiO_2, wet-transferred	7.6	11	0.6	0.87	7.5	8.6/13.1
sample B: grown on Si/SiO_2, wet-transferred	13.7	20	0.38	2.2	1.3	8.7/9.9
sample C: grown on Si/SiO_2, wet-transferred	23.5	34	0.85	7.5	1.6	8.5/9.7
sample D: directly grown on Si waveguide	27	39	1.2	11	1.9	8.4/8.7

[a]A single layer $PtSe_2$ has a thickness of about 0.7 nm.[68] The number of layers for each film can be estimated accordingly. [b]Reported at 4.5 V bias voltage.

mode fiber. The fiber-to-fiber losses of the grating couplers and the waveguides of 8 dB were measured on separate test structures and subtracted to obtain these values. First, we measured the specific absorption of the evanescent field by the $PtSe_2$ films located at 10 nm distance to the waveguide using structures with different $PtSe_2$ dimensions (Figure 2c). The resulting absorption was 0.06, 0.38, 0.85, and 1.2 dB/μm for 7.6, 13.7, 23.5, and 27 nm $PtSe_2$, respectively.

The opto-electric response of the $PtSe_2$ PDs was investigated by measuring the photocurrents with a lock-in amplifier while modulating the light intensity at a frequency of 1 kHz (see also the Supporting Information). The photocurrents were measured as a function of laser light power for each PD with a width of 50 μm (along the waveguides) and a length of 13 μm (perpendicular to the waveguides, i.e., distance between the contacts) for an applied bias voltage of V_{ds} = 4.5 V across the device. All detectors exhibit a linear dependence on light power for the measured range. The highest photocurrent is observed for the device with the thickest $PtSe_2$ film which is directly grown on the waveguide (Figure 3a). The intrinsic responsivity is defined as $R = I_{ph}/P_{opt}$, where I_{ph} is the photocurrent and P_{opt} is the optical power arriving at the PD after subtracting the losses of the grating couplers and waveguides. Measurements of the responsivities at different

https://doi.org/10.1021/acsphotonics.1c01517
ACS Photonics 2022, 9, 859−867

Table 2. Characteristics and Performance Metrics of PDs Based on 2D Materials

materials	growth methods	wavelength	responsivity	response time	ref
graphene	CVD	1550 nm	180 mA/W	2.7 ps[a]	73
BP	exfoliation	3.8 μm	11.3 A/W	0.3 ms	74
MoS_2	MOVPE	360−960 nm	920 A/W	0.5/1.15 s	57
MoS_2	exfoliation	980 nm	2.3 A/W	50 ms	19
HfS_2	CVD	808	3.8×10^5 A/W	8 ms	75
$MoTe_2$	CVD	980	6.4 A/W	31/21 ms	76
$MoTe_2$/Gr	exfoliation	1300 nm	0.2 A/W	7 ps[a]	77
$PtSe_2$	TAC	635−2.7 μm	7.8 mA/W	6/9 μs	36
$PtSe_2$	CVD	1550 nm	0.19 mA/W	17/39 ps	78
$PtSe_2$	TAC	1550 nm	11 mA/W	8.4/8.7 μs	this work

[a]Calculated from the reported 3 dB bandwidth.

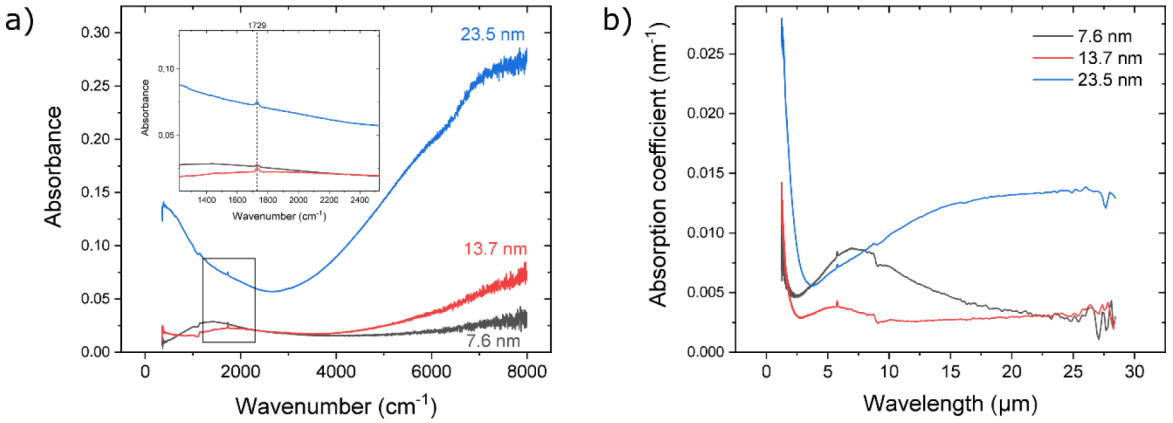

Figure 4. (a) Absorbance of $PtSe_2$ using FTIR spectroscopy. Inset: magnified view of the peak at 1729 cm^{-1} (5784 nm). (b) Absorption coefficients of $PtSe_2$ films with different thicknesses, calculated from their absorbance.

bias voltages ranging from $V_{ds} = -4.5$ to 4.5 V at a fixed laser output power of 9 mW are plotted in Figure 3b. Increasing V_{ds} results in higher photocurrents and consequently higher responsivities. At 4.5 V applied bias voltage, this intrinsic responsivity yields $R = 0.8$ mA/W for the thinnest $PtSe_2$ layer (7.6 nm) up to a maximum value of $R = 11$ mA/W for the PD with a directly grown $PtSe_2$ layer of 27 nm thickness (Table 1). Different devices on each chip were measured and statistics of the responsivities are also shown in Figure 3c, which confirms that the responsivity of the devices increases with the number of $PtSe_2$ layers.

The normalized photocurrent-to-dark current ratio (NPDR), defined as responsivity divided by the dark current, is another important parameter for evaluating the sensitivity of the PDs. Larger NPDR values indicate better suppression of dark currents and lower noise-equivalent power. The NPDRs of all the PDs have been calculated and listed in Table 1. The NPDR values for the $PtSe_2$ PDs are similar to those reported for graphene PDs but have the strong advantage of enabling direct growth instead of transfer.[22,54]

Time-resolved measurements were performed on the $PtSe_2$ PDs (Figure 3d). The rise and fall times are defined by the time it takes for the photocurrent to reach 10 and 90% of the maximum value in rising and decaying curves, respectively, or by fitting eqs 1 and 2:[55]

$$I_{rise} = I_0 + Ae^{(t-t_1/\tau)} \quad (1)$$

$$I_{fall} = I_0 + Be^{(-t-t_2/\tau)} \quad (2)$$

where τ is the rise/fall time constant and t_1 or t_2 is the time it takes for switching the laser on or off, respectively. The measured rise and fall times for the PDs are listed in Table 1. The values for all the detectors are between 8 and 13 μs. Consequently, our PDs provide a faster response time than most of the reported TMD-based IR PDs so far.[56,57] The performance parameters of merit for some 2D-based IR PDs are summarized in Table 2. The transient time (τ_t), that is, the time needed for the photocarriers to reach the metal contacts, can be calculated through the carrier drift model by eq 3:[58]

$$\tau_t = \frac{L^2}{2\mu V_{ds}} \quad (3)$$

where L is the length of the channel perpendicular to the propagation of the light, μ is the electron mobility, and V_{ds} is the applied bias. To approximate the carrier mobility, $PtSe_2$ films with the same thicknesses as used for the PDs and grown in the same batch were wet-transferred onto a Si substrate with the 90 nm SiO_2 layer. After fabrication of the contacts and patterning of the PSe_2 films, the field-effect mobility of all the film thicknesses was calculated using the transconductance method in eq 4:[59,60]

$$\mu = g_m \frac{L}{WV_{ds}C_g} \quad (4)$$

Here, W is the channel width along the waveguide and V_{ds} is the voltage applied to the device channel. g_m is defined as $\frac{dI_{ds}}{dV_g}$, where I_{ds} is the drain-source current and V_g is the back-gate

https://doi.org/10.1021/acsphotonics.1c01517
ACS Photonics 2022, 9, 859−867

voltage, and $C_g = \frac{\varepsilon\varepsilon_0}{t_{ox}}$ is the back-gate capacitance of SiO_2. ε and ε_0 are the relative and vacuum permittivity and t_{ox} is the thickness of SiO_2. The extracted field-effect mobilities for all $PtSe_2$ films were between 2.7 and 3.9 cm^2/Vs. This relatively low value can be attributed to defects and the polycrystallinity of the films grown by the TAC method.[39,47] Literature data on mobilities of $PtSe_2$ films show broad variability ranging from values below 1 cm^2/Vs for TAC-grown films[42,61,62] to 210 cm^2/Vs for exfoliated films.[38] Most of the studies report mobilities below 50 cm^2/Vs.[63−67] Using the extracted carrier mobility, the transient time for a device with L = 13 μm and 4.5 V bias voltage is 0.6 ns.

Potential applications for photonic-integrated IR PDs beyond the telecommunication wavelengths are sensing, diagnostics, thermal imaging, and free space communication.[60,69] Therefore, we have studied the broadband absorption of $PtSe_2$ films with different thicknesses for the wavelength range from 1.2 to 28 μm using Fourier-transform IR (FTIR) spectroscopy. We wet-transferred $PtSe_2$ films with thicknesses of 7.6, 13.7, and 23.5 nm onto separate Si substrates and measured their absorbance (A) by FTIR spectroscopy while subtracting the absorbance of the Si substrate (Figure 4a). All $PtSe_2$ films exhibit a small peak at 1729 cm^{-1} (5784 nm). The absorption coefficients (α) of the $PtSe_2$ films were also calculated from their absorbance by eq 5,

$$A\ln(10) = \alpha t \tag{5}$$

where A is the absorbance of the material and t is the film's thickness (Figure 4b). The absorption coefficient of the sample with the thickest $PtSe_2$ (23.5 nm) layer behaves differently from the other two samples: while its absorption decreases at first in a similar way to the 7.6 and 13.7 nm thick films, it starts to increase to a steady value as the wavelength increases further. The coefficients of the thinner films remain low as the wavelength increases. The absorption of the 23.5 nm thick $PtSe_2$ is nonzero even at 28 μm wavelength (0.04 eV) which can be considered metallic behavior.[70] This result suggests that $PtSe_2$ may also be suitable for long-wavelength mid-IR PDs.

We have demonstrated the integration of $PtSe_2$ PDs into silicon photonic waveguides and demonstrated their functionality at a wavelength of 1550 nm. We have shown that layered $PtSe_2$ can be utilized for IR photodetection with high responsivity. Our $PtSe_2$ PDs can be synthesized directly on the photonic waveguide structures, on wafer scale, and at CMOS-compatible temperatures using TAC. The directly grown films show higher performance than reference devices transferred with a typical 2D layer-transfer method. The highest responsivity of 11 mA/W was achieved for a directly grown $PtSe_2$ PD, which reached a fast response time of 8.4 μs. FTIR data indicate that $PtSe_2$ is suitable for photodetection well into the mid-IR range, which opens opportunities for applications in food safety, agriculture, gas detection, on-chip spectroscopy, or imaging. The direct growth of $PtSe_2$ on waveguides creates a new perspective for the integration of 2D materials with PICs. Our results show that multilayered $PtSe_2$ is a promising candidate for high-responsivity optoelectronic applications in the near- and mid-IR regime, including the direct integration on commercial semiconductor technology platforms. This includes silicon nitride (SiN) photonics as the growth methods do not require any crystalline surfaces, in contrast to epitaxial processes.[40,66,71,72]

METHODS

Device fabrication: Silicon rib waveguides with a 50 nm step height were fabricated on a 150 mm SOI wafer with 220 nm top Si and 3 μm buried oxide layers using i-line (365 nm) photolithography and reactive ion etching (RIE). Grating couplers designed for the 1550 nm wavelength were realized at the end of the waveguides by electron beam lithography and subsequent RIE. 10 nm of Al_2O_3 was deposited on the wafer by ALD to protect the waveguides and grating couplers from the diffusion of Pt into the top Si layer during the growth process and also to avoid the formation of a Schottky junction between $PtSe_2$ and the bottom Si. The thin Al_2O_3 works as a cladding for grating couplers and increases their coupling efficiency.

The SOI wafer was diced after fabricating the photonic base components, and $PtSe_2$ PDs were fabricated on different dies of the wafer.

For the directly grown sample, a 10.8 nm Pt layer was sputtered onto the waveguides using a predefined lithography pattern and a lift-off process. The Pt layer was converted into $PtSe_2$ of 27 nm thickness. $PtSe_2$ films with thicknesses of 7.6, 13.7, and 23.5 nm were grown on separate Si/SiO_2 (90 nm) substrates and then wet-transferred onto the separate samples using potassium hydroxide (KOH) solution. All $PtSe_2$ films were grown using this TAC process, as described in detail in previous publications.[34,49] For wet transfer, a support layer of poly(methyl methacrylate) (PMMA) was spin-coated on top of the $PtSe_2$ films. Then, the PMMA film was scratched, and a few droplets of KOH solution were dropped on the scratched areas. KOH causes delamination of $PtSe_2$ films from underlying SiO_2. After delamination and release of $PtSe_2$/PMMA films from the substrates, they remained floating on the deionized water for few days and then were transferred onto the final substrates using the fishing technique. The samples were dried in air, and then the PMMA layer was removed from their surfaces using acetone and isopropanol. The transferred $PtSe_2$ films were patterned using contact lithography and RIE. Afterward, all $PtSe_2$ films came in contact with 15 nm Ni and 50 nm Al using contact lithography and a subsequent lift-off process.

Electrical characterization: Electrical measurements were performed in a Lakeshore chamber connected to a Keithley SCS4200 source meter unit under ambient conditions.

FTIR measurements: The absorption spectra were calculated from transmittance measurements. The data were recorded from 0.05 eV (400 cm^{-1}) up to 0.99 eV (8000 cm^{-1}) using a Bruker Vertex 80v Fourier-transform spectrometer with a spectral resolution of 0.5 meV (4 cm^{-1}) and averaged over 64 scans.

ASSOCIATED CONTENT

Supporting Information

The Supporting Information is available free of charge at https://pubs.acs.org/doi/10.1021/acsphotonics.1c01517.

Thickness measurements of $PtSe_2$ films using AFM, more details about opto-electrical measurements and setup, and comments on IV curve characteristics (PDF)

AUTHOR INFORMATION

Corresponding Authors

Stephan Suckow − *AMO GmbH, Advanced Microelectronic Center Aachen, 52074 Aachen, Germany;* orcid.org/0000-0002-1116-169X; Email: suckow@amo.de

https://doi.org/10.1021/acsphotonics.1c01517
ACS Photonics 2022, 9, 859−867

Max C. Lemme − *Chair of Electronic Devices, RWTH Aachen University, 52074 Aachen, Germany; AMO GmbH, Advanced Microelectronic Center Aachen, 52074 Aachen, Germany;* orcid.org/0000-0003-4552-2411; Email: max.lemme@eld.rwth-aachen.de

Authors

Shayan Parhizkar − *Chair of Electronic Devices, RWTH Aachen University, 52074 Aachen, Germany; AMO GmbH, Advanced Microelectronic Center Aachen, 52074 Aachen, Germany;* orcid.org/0000-0001-7976-1344

Maximilian Prechtl − *Institute of Physics, Faculty of Electrical Engineering and Information Technology (EIT 2) and Center for Integrated Sensor Systems, University of the Bundeswehr Munich, 85577 Neubiberg, Germany*

Anna Lena Giesecke − *AMO GmbH, Advanced Microelectronic Center Aachen, 52074 Aachen, Germany;* orcid.org/0000-0002-3072-4451

Sophia Wahl − *Institute of Physics IA, RWTH Aachen University, 52074 Aachen, Germany*

Sebastian Lukas − *Chair of Electronic Devices, RWTH Aachen University, 52074 Aachen, Germany;* orcid.org/0000-0002-8062-2832

Oliver Hartwig − *Institute of Physics, Faculty of Electrical Engineering and Information Technology (EIT 2) and Center for Integrated Sensor Systems, University of the Bundeswehr Munich, 85577 Neubiberg, Germany*

Nour Negm − *Chair of Electronic Devices, RWTH Aachen University, 52074 Aachen, Germany; AMO GmbH, Advanced Microelectronic Center Aachen, 52074 Aachen, Germany*

Arne Quellmalz − *Division of Micro and Nanosystems, School of Electrical Engineering and Computer Science, KTH Royal Institute of Technology, SE-10044 Stockholm, Sweden;* orcid.org/0000-0003-3936-818X

Kristinn Gylfason − *Division of Micro and Nanosystems, School of Electrical Engineering and Computer Science, KTH Royal Institute of Technology, SE-10044 Stockholm, Sweden;* orcid.org/0000-0001-9008-8402

Daniel Schall − *AMO GmbH, Advanced Microelectronic Center Aachen, 52074 Aachen, Germany; Black Semiconductor GmbH, 52072 Aachen, Germany*

Matthias Wuttig − *Institute of Physics IA, RWTH Aachen University, 52074 Aachen, Germany;* orcid.org/0000-0003-1498-1025

Georg S. Duesberg − *Institute of Physics, Faculty of Electrical Engineering and Information Technology (EIT 2) and Center for Integrated Sensor Systems, University of the Bundeswehr Munich, 85577 Neubiberg, Germany;* orcid.org/0000-0002-7412-700X

Complete contact information is available at: https://pubs.acs.org/10.1021/acsphotonics.1c01517

Funding

This work has received funding from the European Union's Horizon 2020 research and innovation programme under grant agreements 825272 (ULISSES) and 881603 (Graphene Flagship Core 3), as well as the German Ministry of Education and Research (BMBF) under grant agreement 16ES1121 (ForMikro-NobleNEMS).

Notes

The authors declare no competing financial interest.

REFERENCES

(1) Rahim, A.; Goyvaerts, J.; Szelag, B.; Fedeli, J.-M.; Absil, P.; Aalto, T.; Harjanne, M.; Littlejohns, C.; Reed, G.; Winzer, G.; Lischke, S.; Zimmermann, L.; Knoll, D.; Geuzebroek, D.; Leinse, A.; Geiselmann, M.; Zervas, M.; Jans, H.; Stassen, A.; Domínguez, C.; Muñoz, P.; Domenech, D.; Giesecke, A. L.; Lemme, M. C.; Baets, R. Open-Access Silicon Photonics Platforms in Europe. *IEEE J. Sel. Top. Quantum Electron.* **2019**, *25*, 1−18.

(2) Geis, M. W.; Spector, S. J.; Grein, M. E.; Yoon, J. U.; Lennon, D. M.; Lyszczarz, T. M. Silicon Waveguide Infrared Photodiodes with >35 GHz Bandwidth and Phototransistors with 50 AW-1 Response. *Opt. Express* **2009**, *17*, 5193−5204.

(3) Liu, J.; Michel, J.; Giziewicz, W.; Pan, D.; Wada, K.; Cannon, D. D.; Jongthammanurak, S.; Danielson, D. T.; Kimerling, L. C.; Chen, J.; Ilday, F. Ö.; Kärtner, F. X.; Yasaitis, J. High-Performance, Tensile-Strained Ge p-i-n Photodetectors on a Si Platform. *Appl. Phys. Lett.* **2005**, *87*, 103501.

(4) Sheng, Z.; Liu, L.; Brouckaert, J.; He, S.; Van Thourhout, D. InGaAs PIN Photodetectors Integrated on Silicon-on-Insulator Waveguides. *Opt. Express* **2010**, *18*, 1756−1761.

(5) Rogalski, A. HgCdTe Infrared Detector Material: History, Status and Outlook. *Rep. Prog. Phys.* **2005**, *68*, 2267−2336.

(6) Konstantatos, G. Current Status and Technological Prospect of Photodetectors Based on Two-Dimensional Materials. *Nat. Commun.* **2018**, *9*, 5266.

(7) Wang, F.; Zhang, Y.; Gao, Y.; Luo, P.; Su, J.; Han, W.; Liu, K.; Li, H.; Zhai, T. 2D Metal Chalcogenides for IR Photodetection. *Small* **2019**, *15*, No. 1901347.

(8) Koppens, F. H. L.; Mueller, T.; Avouris, P.; Ferrari, A. C.; Vitiello, M. S.; Polini, M. Photodetectors Based on Graphene, Other Two-Dimensional Materials and Hybrid Systems. *Nat. Nanotechnol.* **2014**, *9*, 780−793.

(9) Bablich, A.; Kataria, S.; Lemme, M. C. Graphene and Two-Dimensional Materials for Optoelectronic Applications. *Electronics* **2016**, *5*, 13.

(10) Xia, F.; Wang, H.; Xiao, D.; Dubey, M.; Ramasubramaniam, A. Two-Dimensional Material Nanophotonics. *Nat. Photonics* **2014**, *8*, 899−907.

(11) Liu, C.; Zheng, J.; Chen, Y.; Fryett, T.; Majumdar, A. Van Der Waals Materials Integrated Nanophotonic Devices [Invited]. *Opt. Mater. Express* **2019**, *9*, 384−399.

(12) Yu, X.; Yu, P.; Wu, D.; Singh, B.; Zeng, Q.; Lin, H.; Zhou, W.; Lin, J.; Suenaga, K.; Liu, Z.; Wang, Q. J. Atomically Thin Noble Metal Dichalcogenide: A Broadband Mid-Infrared Semiconductor. *Nat. Commun.* **2018**, *9*, 1545.

(13) Sun, Z.; Martinez, A.; Wang, F. Optical Modulators with 2D Layered Materials. *Nat. Photonics* **2016**, *10*, 227−238.

(14) Jakhar, A.; Kumar, P.; Moudgil, A.; Dhyani, V.; Das, S. Optically Pumped Broadband Terahertz Modulator Based on Nanostructured $PtSe_2$ Thin Films. *Adv. Opt. Mater.* **2020**, *8*, No. 1901714.

(15) Yuan, J.; Mu, H.; Li, L.; Chen, Y.; Yu, W.; Zhang, K.; Sun, B.; Lin, S.; Li, S.; Bao, Q. Few-Layer Platinum Diselenide as a New Saturable Absorber for Ultrafast Fiber Lasers. *ACS Appl. Mater. Interfaces* **2018**, *10*, 21534−21540.

(16) Pospischil, A.; Furchi, M. M.; Mueller, T. Solar-Energy Conversion and Light Emission in an Atomic Monolayer p−n Diode. *Nat. Nanotechnol.* **2014**, *9*, 257−261.

(17) Lee, H. S.; Min, S.-W.; Chang, Y.-G.; Park, M. K.; Nam, T.; Kim, H.; Kim, J. H.; Ryu, S.; Im, S. MoS2 Nanosheet Phototransistors with Thickness-Modulated Optical Energy Gap. *Nano Lett.* **2012**, *12*, 3695−3700.

(18) Choi, W.; Cho, M. Y.; Konar, A.; Lee, J. H.; Cha, G.-B.; Hong, S. C.; Kim, S.; Kim, J.; Jena, D.; Joo, J.; Kim, S. High-Detectivity Multilayer MoS2 Phototransistors with Spectral Response from Ultraviolet to Infrared. *Adv. Mater.* **2012**, *24*, 5832−5836.

(19) Wu, J.-Y.; Chun, Y. T.; Li, S.; Zhang, T.; Wang, J.; Shrestha, P. K.; Chu, D. Broadband MoS2 Field-Effect Phototransistors: Ultra-

sensitive Visible-Light Photoresponse and Negative Infrared Photoresponse. *Adv. Mater.* **2018**, *30*, No. 1705880.
(20) Seo, J.; Lee, J. H.; Pak, J.; Cho, K.; Kim, J.-K.; Kim, J.; Jang, J.; Ahn, H.; Lim, S. C.; Chung, S.; Kang, K.; Lee, T. Ultrasensitive Photodetection in MoS2 Avalanche Phototransistors. *Adv. Sci.* **2021**, *8*, No. 2102437.
(21) Liu, M.; Yin, X.; Ulin-Avila, E.; Geng, B.; Zentgraf, T.; Ju, L.; Wang, F.; Zhang, X. A Graphene-Based Broadband Optical Modulator. *Nature* **2011**, *474*, 64−67.
(22) Wang, X.; Cheng, Z.; Xu, K.; Tsang, H. K.; Xu, J.-B. High-Responsivity Graphene/Silicon-Heterostructure Waveguide Photodetectors. *Nat. Photonics* **2013**, *7*, 888−891.
(23) Pospischil, A.; Humer, M.; Furchi, M. M.; Bachmann, D.; Guider, R.; Fromherz, T.; Mueller, T. CMOS-Compatible Graphene Photodetector Covering All Optical Communication Bands. *Nat. Photonics* **2013**, *7*, 892−896.
(24) Schall, D.; Neumaier, D.; Mohsin, M.; Chmielak, B.; Bolten, J.; Porschatis, C.; Prinzen, A.; Matheisen, C.; Kuebart, W.; Junginger, B.; Templ, W.; Giesecke, A. L.; Kurz, H. 50 GBit/s Photodetectors Based on Wafer-Scale Graphene for Integrated Silicon Photonic Communication Systems. *ACS Photonics* **2014**, *1*, 781−784.
(25) Romagnoli, M.; Sorianello, V.; Midrio, M.; Koppens, F. H. L.; Huyghebaert, C.; Neumaier, D.; Galli, P.; Templ, W.; D'Errico, A.; Ferrari, A. C. Graphene-Based Integrated Photonics for next-Generation Datacom and Telecom. *Nat. Rev. Mater.* **2018**, *3*, 392−414.
(26) Neumaier, D.; Pindl, S.; Lemme, M. C. Integrating Graphene into Semiconductor Fabrication Lines. *Nat. Mater.* **2019**, *18*, 525−529.
(27) Quellmalz, A.; Wang, X.; Sawallich, S.; Uzlu, B.; Otto, M.; Wagner, S.; Wang, Z.; Prechtl, M.; Hartwig, O.; Luo, S.; Duesberg, G. S.; Lemme, M. C.; Gylfason, K. B.; Roxhed, N.; Stemme, G.; Niklaus, F. Large-Area Integration of Two-Dimensional Materials and Their Heterostructures by Wafer Bonding. *Nat. Commun.* **2021**, *12*, 917.
(28) Engel, M.; Steiner, M.; Avouris, P. Black Phosphorus Photodetector for Multispectral, High-Resolution Imaging. *Nano Lett.* **2014**, *14*, 6414−6417.
(29) Buscema, M.; Groenendijk, D. J.; Blanter, S. I.; Steele, G. A.; van der Zant, H. S. J.; Castellanos-Gomez, A. Fast and Broadband Photoresponse of Few-Layer Black Phosphorus Field-Effect Transistors. *Nano Lett.* **2014**, *14*, 3347−3352.
(30) Huang, L.; Dong, B.; Guo, X.; Chang, Y.; Chen, N.; Huang, X.; Liao, W.; Zhu, C.; Wang, H.; Lee, C.; Ang, K.-W. Waveguide-Integrated Black Phosphorus Photodetector for Mid-Infrared Applications. *ACS Nano* **2019**, *13*, 913−921.
(31) Youngblood, N.; Chen, C.; Koester, S. J.; Li, M. Waveguide-Integrated Black Phosphorus Photodetector with High Responsivity and Low Dark Current. *Nat. Photonics* **2015**, *9*, 247−252.
(32) Illarionov, Y. Y.; Waltl, M.; Rzepa, G.; Kim, J.-S.; Kim, S.; Dodabalapur, A.; Akinwande, D.; Grasser, T. Long-Term Stability and Reliability of Black Phosphorus Field-Effect Transistors. *ACS Nano* **2016**, *10*, 9543−9549.
(33) Miró, P.; Ghorbani-Asl, M.; Heine, T. Two Dimensional Materials Beyond MoS2: Noble-Transition-Metal Dichalcogenides. *Angew. Chem., Int. Ed.* **2014**, *53*, 3015−3018.
(34) Yim, C.; Lee, K.; McEvoy, N.; O'Brien, M.; Riazimehr, S.; Berner, N. C.; Cullen, C. P.; Kotakoski, J.; Meyer, J. C.; Lemme, M. C.; Duesberg, G. S. High-Performance Hybrid Electronic Devices from Layered PtSe2 Films Grown at Low Temperature. *ACS Nano* **2016**, *10*, 9550−9558.
(35) Yim, C.; McEvoy, N.; Riazimehr, S.; Schneider, D. S.; Gity, F.; Monaghan, S.; Hurley, P. K.; Lemme, M. C.; Duesberg, G. S. Wide Spectral Photoresponse of Layered Platinum Diselenide-Based Photodiodes. *Nano Lett.* **2018**, *18*, 1794−1800.
(36) Zhou, K.; Shen, J.; Li, X.; Hong, X.; Feng, W.; Tang, X.; Jiang, X.; Wei, D.; Chen, Y.; Liu, X.; Xie, Y.; Wei, D.; Sun, T. Broadband Photodetector Based on 2D Layered PtSe2/Silicon Heterojunction at Room-Temperature. *Phys. E* **2020**, *123*, No. 114147.
(37) Zhang, W.; Huang, Z.; Zhang, W.; Li, Y. Two-Dimensional Semiconductors with Possible High Room Temperature Mobility. *Nano Res.* **2014**, *7*, 1731−1737.
(38) Zhao, Y.; Qiao, J.; Yu, Z.; Yu, P.; Xu, K.; Lau, S. P.; Zhou, W.; Liu, Z.; Wang, X.; Ji, W.; Chai, Y. High-Electron-Mobility and Air-Stable 2D Layered PtSe2 FETs. *Adv. Mater.* **2017**, *29*, No. 1604230.
(39) Wagner, S.; Yim, C.; McEvoy, N.; Kataria, S.; Yokaribas, V.; Kuc, A.; Pindl, S.; Fritzen, C.-P.; Heine, T.; Duesberg, G. S.; Lemme, M. C. Highly Sensitive Electromechanical Piezoresistive Pressure Sensors Based on Large-Area Layered PtSe2 Films. *Nano Lett.* **2018**, *18*, 3738−3745.
(40) Boland, C. S.; Coileáin, C. Ó.; Wagner, S.; McManus, J. B.; Cullen, C. P.; Lemme, M. C.; Duesberg, G. S.; McEvoy, N. PtSe 2 Grown Directly on Polymer Foil for Use as a Robust Piezoresistive Sensor. *2D Mater.* **2019**, *6*, No. 045029.
(41) Lukas, S.; Hartwig, O.; Prechtl, M.; Capraro, G.; Bolten, J.; Meledin, A.; Mayer, J.; Neumaier, D.; Kataria, S.; Duesberg, G. S.; Lemme, M. C. Correlating Nanocrystalline Structure with Electronic Properties in 2D Platinum Diselenide. *Adv. Funct. Mater.* **2021**, *31*, No. 2102929.
(42) Yim, C.; Passi, V.; Lemme, M. C.; Duesberg, G. S.; Ó Coileáin, C.; Pallecchi, E.; Fadil, D.; McEvoy, N. Electrical Devices from Top-down Structured Platinum Diselenide Films. *Npj 2D Mater. Appl.* **2018**, *2*, 5.
(43) Ansari, L.; Monaghan, S.; McEvoy, N.; Coileáin, C. Ó.; Cullen, C. P.; Lin, J.; Siris, R.; Stimpel-Lindner, T.; Burke, K. F.; Mirabelli, G.; Duffy, R.; Caruso, E.; Nagle, R. E.; Duesberg, G. S.; Hurley, P. K.; Gity, F. Quantum Confinement-Induced Semimetal-to-Semiconductor Evolution in Large-Area Ultra-Thin PtSe2 Films Grown at 400 °C. *Npj 2D Mater. Appl.* **2019**, *3*, 33.
(44) Prechtl, M.; Parhizkar, S.; Hartwig, O.; Lee, K.; Biba, J.; Stimpel-Lindner, T.; Gity, F.; Schels, A.; Bolten, J.; Suckow, S.; Giesecke, A. L.; Lemme, M. C.; Duesberg, G. S. Hybrid Devices by Selective and Conformal Deposition of PtSe2 at Low Temperatures. *Adv. Funct. Mater.* **2021**, *31*, No. 2103936.
(45) Vaziri, S.; Smith, A. D.; Östling, M.; Lupina, G.; Dabrowski, J.; Lippert, G.; Mehr, W.; Driussi, F.; Venica, S.; Di Lecce, V.; Gnudi, A.; König, M.; Ruhl, G.; Belete, M.; Lemme, M. C. Going Ballistic: Graphene Hot Electron Transistors. *Solid State Commun.* **2015**, *224*, 64−75.
(46) Phare, C. T.; Daniel Lee, Y.-H.; Cardenas, J.; Lipson, M. Graphene Electro-Optic Modulator with 30 GHz Bandwidth. *Nat. Photonics* **2015**, *9*, 511−514.
(47) Maiti, R.; Patil, C.; Saadi, M. A. S. R.; Xie, T.; Azadani, J. G.; Uluutku, B.; Amin, R.; Briggs, A. F.; Miscuglio, M.; Van Thourhout, D.; Solares, S. D.; Low, T.; Agarwal, R.; Bank, S. R.; Sorger, V. J. Strain-Engineered High-Responsivity MoTe2 Photodetector for Silicon Photonic Integrated Circuits. *Nat. Photonics* **2020**, *14*, 578−584.
(48) Zhang, W.; Qin, J.; Huang, Z.; Zhang, W. The Mechanism of Layer Number and Strain Dependent Bandgap of 2D Crystal PtSe2. *J. Appl. Phys.* **2017**, *122*, 205701.
(49) O'Brien, M.; McEvoy, N.; Motta, C.; Zheng, J.-Y.; Berner, N. C.; Kotakoski, J.; Elibol, K.; Pennycook, T. J.; Meyer, J. C.; Yim, C.; Abid, M.; Hallam, T.; Donegan, J. F.; Sanvito, S.; Duesberg, G. S. Raman Characterization of Platinum Diselenide Thin Films. *2D Mater.* **2016**, *3*, No. 021004.
(50) Jiang, W.; Wang, X.; Chen, Y.; Wu, G.; Ba, K.; Xuan, N.; Sun, Y.; Gong, P.; Bao, J.; Shen, H.; Lin, T.; Meng, X.; Wang, J.; Sun, Z. Large-Area High Quality PtSe2 Thin Film with Versatile Polarity. *InfoMat* **2019**, *1*, 260−267.
(51) Szydlowska, B. M.; Hartwig, O.; Tywoniuk, B.; Hartman, T.; Stimpel-Lindner, T.; Sofer, Z.; McEvoy, N.; Duesberg, G. S.; Backes, C. Spectroscopic Thickness and Quality Metrics for PtSe2 Layers Produced by Top-down and Bottom-up Techniques. *2D Mater.* **2020**, *7*, No. 045027.
(52) Das, T.; Yang, E.; Seo, J. E.; Kim, J. H.; Park, E.; Kim, M.; Seo, D.; Kwak, J. Y.; Chang, J. Doping-Free All PtSe2 Transistor via

Thickness-Modulated Phase Transition. *ACS Appl. Mater. Interfaces* **2021**, *13*, 1861−1871.
(53) Xie, J.; Zhang, D.; Yan, X.-Q.; Ren, M.; Zhao, X.; Liu, F.; Sun, R.; Li, X.; Li, Z.; Chen, S.; Liu, Z.-B.; Tian, J.-G. Optical Properties of Chemical Vapor Deposition-Grown PtSe 2 Characterized by Spectroscopic Ellipsometry. *2D Mater.* **2019**, *6*, No. 035011.
(54) Guo, J.; Li, J.; Liu, C.; Yin, Y.; Wang, W.; Ni, Z.; Fu, Z.; Yu, H.; Xu, Y.; Shi, Y.; Ma, Y.; Gao, S.; Tong, L.; Dai, D. High-Performance Silicon−graphene Hybrid Plasmonic Waveguide Photodetectors beyond 1.55 Mm. *Light: Sci. Appl.* **2020**, *9*, 29.
(55) Island, J. O.; Buscema, M.; Barawi, M.; Clamagirand, J. M.; Ares, J. R.; Sánchez, C.; Ferrer, I. J.; Steele, G. A.; van der Zant, H. S. J.; Castellanos-Gomez, A. Ultrahigh Photoresponse of Few-Layer TiS3 Nanoribbon Transistors. *Adv. Opt. Mater.* **2014**, *2*, 641−645.
(56) Gong, Y.; Lin, Z.; Chen, Y.-X.; Khan, Q.; Wang, C.; Zhang, B.; Nie, G.; Xie, N.; Li, D. Two-Dimensional Platinum Diselenide: Synthesis, Emerging Applications, and Future Challenges. *Nano-Micro Lett.* **2020**, *12*, 174.
(57) Schneider, D. S.; Grundmann, A.; Bablich, A.; Passi, V.; Kataria, S.; Kalisch, H.; Heuken, M.; Vescan, A.; Neumaier, D.; Lemme, M. C. Highly Responsive Flexible Photodetectors Based on MOVPE Grown Uniform Few-Layer MoS2. *ACS Photonics* **2020**, *7*, 1388−1395.
(58) Massicotte, M.; Schmidt, P.; Vialla, F.; Schädler, K. G.; Reserbat-Plantey, A.; Watanabe, K.; Taniguchi, T.; Tielrooij, K. J.; Koppens, F. H. L. Picosecond Photoresponse in van Der Waals Heterostructures. *Nat. Nanotechnol.* **2016**, *11*, 42−46.
(59) Zhong, H.; Zhang, Z.; Xu, H.; Qiu, C.; Peng, L.-M. Comparison of Mobility Extraction Methods Based on Field-Effect Measurements for Graphene. *AIP Adv.* **2015**, *5*, No. 057136.
(60) Jing, X.; Illarionov, Y.; Yalon, E.; Zhou, P.; Grasser, T.; Shi, Y.; Lanza, M. Engineering Field Effect Transistors with 2D Semiconducting Channels: Status and Prospects. *Adv. Funct. Mater.* **2020**, *30*, No. 1901971.
(61) Xiong, K.; Hilse, M.; Li, L.; Göritz, A.; Lisker, M.; Wietstruck, M.; Kaynak, M.; Engel-Herbert, R.; Madjar, A.; Hwang, J. C. M. Large-Scale Fabrication of Submicrometer-Gate-Length MOSFETs With a Trilayer PtSe2 Channel Grown by Molecular Beam Epitaxy. *IEEE Trans. Electron Devices* **2020**, *67*, 796−801.
(62) Su, T.-Y.; Medina, H.; Chen, Y.-Z.; Wang, S.-W.; Lee, S.-S.; Shih, Y.-C.; Chen, C.-W.; Kuo, H.-C.; Chuang, F.-C.; Chueh, Y.-L. Phase-Engineered PtSe2-Layered Films by a Plasma-Assisted Selenization Process toward All PtSe2-Based Field Effect Transistor to Highly Sensitive, Flexible, and Wide-Spectrum Photoresponse Photodetectors. *Small* **2018**, *14*, No. 1800032.
(63) Urban, F.; Gity, F.; Hurley, P. K.; McEvoy, N.; Di Bartolomeo, A. Isotropic Conduction and Negative Photoconduction in Ultrathin PtSe2 Films. *Appl. Phys. Lett.* **2020**, *117*, 193102.
(64) Grillo, A.; Faella, E.; Pelella, A.; Giubileo, F.; Ansari, L.; Gity, F.; Hurley, P. K.; McEvoy, N.; Di Bartolomeo, A. Coexistence of Negative and Positive Photoconductivity in Few-Layer PtSe2 Field-Effect Transistors. *Adv. Funct. Mater.* **2021**, *31*, No. 2105722.
(65) Ciarrocchi, A.; Avsar, A.; Ovchinnikov, D.; Kis, A. Thickness-Modulated Metal-to-Semiconductor Transformation in a Transition Metal Dichalcogenide. *Nat. Commun.* **2018**, *9*, 919.
(66) Zhang, K.; Wang, M.; Zhou, X.; Wang, Y.; Shen, S.; Deng, K.; Peng, H.; Li, J.; Lai, X.; Zhang, L.; Wu, Y.; Duan, W.; Yu, P.; Zhou, S. Growth of Large Scale PtTe, PtTe2 and PtSe2 Films on a Wide Range of Substrates. *Nano Res.* **2021**, *14*, 1663−1667.
(67) Xu, H.; Zhang, H.; Liu, Y.; Zhang, S.; Sun, Y.; Guo, Z.; Sheng, Y.; Wang, X.; Luo, C.; Wu, X.; Wang, J.; Hu, W.; Xu, Z.; Sun, Q.; Zhou, P.; Shi, J.; Sun, Z.; Zhang, D. W.; Bao, W. Controlled Doping of Wafer-Scale PtSe2 Films for Device Application. *Adv. Funct. Mater.* **2019**, *29*, No. 1805614.
(68) Wang, Z.; Li, Q.; Besenbacher, F.; Dong, M. Facile Synthesis of Single Crystal PtSe2 Nanosheets for Nanoscale Electronics. *Adv. Mater.* **2016**, *28*, 10224−10229.
(69) Hu, T.; Dong, B.; Luo, X.; Liow, T.-Y.; Song, J.; Lee, C.; Lo, G.-Q. Silicon Photonic Platforms for Mid-Infrared Applications [Invited]. *Photonics Res.* **2017**, *5*, 417−430.
(70) Zhao, X.; Liu, F.; Liu, D.; Yan, X.-Q.; Huo, C.; Hui, W.; Xie, J.; Ye, Q.; Guo, C.; Yao, Y.; Liu, Z.-B.; Tian, J.-G. Thickness-Dependent Ultrafast Nonlinear Absorption Properties of PtSe2 Films with Both Semiconducting and Semimetallic Phases. *Appl. Phys. Lett.* **2019**, *115*, 263102.
(71) Han, S. S.; Kim, J. H.; Noh, C.; Kim, J. H.; Ji, E.; Kwon, J.; Yu, S. M.; Ko, T.-J.; Okogbue, E.; Oh, K. H.; Chung, H.-S.; Jung, Y.; Lee, G.-H.; Jung, Y. Horizontal-to-Vertical Transition of 2D Layer Orientation in Low-Temperature Chemical Vapor Deposition-Grown PtSe2 and Its Influences on Electrical Properties and Device Applications. *ACS Appl. Mater. Interfaces* **2019**, *11*, 13598−13607.
(72) Li, H.; Li, Y.; Aljarb, A.; Shi, Y.; Li, L.-J. Epitaxial Growth of Two-Dimensional Layered Transition-Metal Dichalcogenides: Growth Mechanism, Controllability, and Scalability. *Chem. Rev.* **2018**, *118*, 6134−6150.
(73) Schall, D.; Pallecchi, E.; Ducournau, G.; Avramovic, V.; Otto, M.; Neumaier, D. Record High Bandwidth Integrated Graphene Photodetectors for Communication beyond 180 Gb/s. In *Optical Fiber Communication Conference*; OSA Technical Digest (online); Optical Society of America: San Diego, California, 2018; p M2I.4.
(74) Ma, Y.; Dong, B.; Wei, J.; Chang, Y.; Huang, L.; Ang, K.-W.; Lee, C. High-Responsivity Mid-Infrared Black Phosphorus Slow Light Waveguide Photodetector. *Adv. Opt. Mater.* **2020**, *8*, No. 2000337.
(75) Fu, L.; Wang, F.; Wu, B.; Wu, N.; Huang, W.; Wang, H.; Jin, C.; Zhuang, L.; He, J.; Fu, L.; Liu, Y. Van Der Waals Epitaxial Growth of Atomic Layered HfS2 Crystals for Ultrasensitive Near-Infrared Phototransistors. *Adv. Mater.* **2017**, *29*, No. 1700439.
(76) Yang, D.; Hu, X.; Zhuang, M.; Ding, Y.; Zhou, S.; Li, A.; Yu, Y.; Li, H.; Luo, Z.; Gan, L.; Zhai, T. Inversion Symmetry Broken 2D 3R-MoTe2. *Adv. Funct. Mater.* **2018**, *28*, No. 1800785.
(77) Flöry, N.; Ma, P.; Salamin, Y.; Emboras, A.; Taniguchi, T.; Watanabe, K.; Leuthold, J.; Novotny, L. Waveguide-Integrated van Der Waals Heterostructure Photodetector at Telecom Wavelengths with High Speed and High Responsivity. *Nat. Nanotechnol.* **2020**, *15*, 118−124.
(78) Wang, Y.; Yu, Z.; Tong, Y.; Sun, B.; Zhang, Z.; Xu, J.-B.; Sun, X.; Tsang, H. K. High-Speed Infrared Two-Dimensional Platinum Diselenide Photodetectors. *Appl. Phys. Lett.* **2020**, *116*, 211101.

https://doi.org/10.1021/acsphotonics.1c01517
ACS Photonics 2022, 9, 859−867